Journal of Physics: Conference Series **602** (2015) 012022 doi:10.1088/1742-6596/602/1/012022

A new numerical framework to simulate viscoelastic free-surface flows with the finite-volume method

R Comminal[1,*], J Spangenberg[1,2] and J H Hattel[1]

[1] Department of Mechanical Engineering, Technical University of Denmark, 2800 Kgs. Lyngby, Denmark
[2] Civil and Environmental Engineering, Princeton University, Princeton, NJ-08544, USA

[*] E-mail: rcom@mek.dtu.dkdk

Abstract. A new method for the simulation of 2D viscoelastic flow is presented. Numerical stability is obtained by the logarithmic-conformation change of variable, and a fully-implicit pure-streamfunction flow formulation, without use of any artificial diffusion. As opposed to other simulation results, our calculations predict a hydrodynamic instability in the 4:1 contraction geometry at a Weissenberg number of order 4. This new result is in qualitative agreement with the prediction of a non-linear subcritical elastic instability in Poiseuille flow. Our viscoelastic flow solver is coupled with a volume-of-fluid solver in order to predict free-surfaces in extrusion.

1. Introduction

The numerical simulation of viscoelastic flows with free-surfaces is a relevant problem to the modelling of several shaping processes in the polymer industry, such as extrusion or injection moulding. Polymer melts are typical examples of viscoelastic materials. Such materials can store elastic energy, and have a memory effect. During deformations, the molecular chains get stretched and oriented. As a result, the constitutive behaviour of the material depends on its strain history [1]. In shear flows, the viscoelasticity produces a normal stress difference $\tau_{xx} - \tau_{yy}$. A typical example of a viscoelastic effect happening in the manufacturing industry is the *extrudate swelling*. Another viscoelastic effect is the *elastic turbulence* in curvilinear flows, at very low Reynolds number *Re* (below unity) [2-4]. Recently, Morozov and Saarloos [5] summarized theoretical and experimental evidences of the existence of a *subcritical elastic instability* due to normal stress effects, in planar flows. Linear and non-linear stability analysis [6] showed that the viscoelastic Poiseuille flow is linearly stable at all Weissenberg numbers, but becomes nonlinearly unstable at a Weissenberg number around 4, where the Weissenberg number *Wi* is the dimensionless quantity accounting for the anisotropy created by the normal stress difference:

$$Wi = \left(\tau_{xx} - \tau_{xx}\right)/\tau_{xy}\,, \tag{1}$$

The numerical simulation of viscoelastic flows has for a long time been very challenging, because of the so-called *high Weissenberg number problem* [7]. Numerical investigations show that the simulations are prone to *numerical instability* (divergence of the calculation) for *Wi* above the unity. Another numerical difficulty comes from the resolution of the Navier-Stokes equations at low *Re*,

where classical fractional-step methods lose their efficiency. In this paper, we present a numerical framework which avoids these two difficulties with two changes of variables: the *logarithmic-conformation representation* [8,9], and the *pure-streamfunction flow formulation* [10,11], as described in the section 3. Both reformulations enhance the robustness of the simulation.

When it comes to the modelling of free-surfaces, Lagrangian methods have the advantage to solve directly the position of the surface (coinciding with the position of mesh), without additional calculations, see for instance [12,13]. However, Lagrangian methods become difficult to use when the free-surfaces experience changes of topology, e.g. when surfaces split or merge. For this reason, Eulerian methods are more suitable in general cases. Thus, free-surface problems are typically solved as bi-phasic flows, where one is of the fluid phase is simply air. In the Eulerian methods, the position of the interface between the two phases is represented through the use of an additional discrete variable. We chose to use the *volume-of-fluid* (VOF) method [14], where the additional variable is the volume fraction of the two phases, which is transported with the flow.

2. Governing equations

The governing equations of the viscoelastic flows consist in the continuity equation (conservation of mass)

$$\nabla \cdot \boldsymbol{u} = 0, \tag{2}$$

and the momentum equation (conservation of linear momentum)

$$\rho\left(\frac{\partial \boldsymbol{u}}{\partial t} + \boldsymbol{u}\cdot\nabla\boldsymbol{u}\right) = -\nabla p + \mu_{\mathrm{S}}\nabla^2\boldsymbol{u} + \nabla\cdot\boldsymbol{\sigma}, \tag{3}$$

where $\boldsymbol{u}$ is the velocity vector, p is the isostatic pressure and $\boldsymbol{\sigma}$ the viscoelastic extra-stress tensor. The left hand side in the equation (3) corresponds to the inertial effects; the three terms on the right hand side of equation (3) are the contributions of the pressure gradient, the Newtonian viscous stress of the solvent, and the viscoelastic stress of the polymers, respectively. Finally, the equations of conservation (2)-(3) are supplemented with a constitutive model which closes the system of equations. We use a generic partial-differential viscoelastic model of general form

$$\frac{\partial \boldsymbol{\sigma}}{\partial t} + \boldsymbol{u}\cdot\nabla\boldsymbol{\sigma} - \left(\boldsymbol{\sigma}\cdot\nabla\boldsymbol{u} + \nabla\boldsymbol{u}^{\mathrm{T}}\cdot\boldsymbol{\sigma}\right) + \frac{f(\boldsymbol{\sigma})}{\lambda}\boldsymbol{\sigma} = \frac{2\mu_{\mathrm{P}}}{\lambda}\dot{\boldsymbol{\varepsilon}}, \tag{4}$$

where $f(\boldsymbol{\sigma})$ is a relaxation function, and $\dot{\boldsymbol{\varepsilon}} = (\nabla\boldsymbol{u} + \nabla\boldsymbol{u}^{\mathrm{T}})/2$ is the strain rate tensor. Depending on the expression of $f(\boldsymbol{\sigma})$, popular viscoelastic models can be recovered [1], see table 1. The material parameters ρ, μ_{S}, μ_{P} and λ are the density, the solvent viscosity, the polymer viscosity and the relaxation time, respectively.

Table 1. Expressions of the relaxation function $f(\boldsymbol{\sigma})$ in the generic constitutive equation (4), for different viscoelastic models.

Viscoelastic model	Relaxation function $f(\boldsymbol{\sigma})$
Oldroyd-B	1
Giesekus	$1+(\alpha\lambda/\mu_1)\boldsymbol{\sigma}$
Linear PTT	$1+(\varepsilon\lambda/\mu_1)\,\mathrm{tr}(\boldsymbol{\sigma})$
Exponential PTT	$\exp\left[(\varepsilon\lambda/\mu_1)\,\mathrm{tr}(\boldsymbol{\sigma})\right]$
FENE-CR	$\left[1+(\lambda/\mu_1 L^2)\,\mathrm{tr}(\boldsymbol{\sigma})\right]^{-1}$

3. Numerical framework

The continuum problem is discretized with the finite-volume method, where the governing equations translate to balances of the fluxes between discrete control volumes. The fluxes are evaluated by a *quadratic upwind interpolation* scheme with flux limiters (CUBISTA) introduced by Alves et al. [15]. The equations are integrated in time with the *two-level backward differentiation formula* (BDF2). Our implementation of the VOF method uses the second-order accurate algorithm of Pilliod and Puckett [16], where the piecewise linear approximations of the interface are reconstructed with the ELVIRA technique, and the advection is solved explicitly by an operator split algorithm. Because of the non-linearity, the volume fraction, constitutive and conservation equations are solved sequentially, with successive *direct substitution* iterations until a convergence criterion is reached, at each time-step.

3.1. The log-conformation representation

The log-conformation reformulation of the constitutive equation was recently introduced by Fattal and Kupferman [8,9]. It expresses the viscoelastic extra-stress $\boldsymbol{\sigma}$ in the constitutive equation (4) in terms of the logarithmic conformation $\boldsymbol{s} = \log(\boldsymbol{c})$. The conformation tensor, defined as

$$\boldsymbol{c} = (\lambda/\mu_{\mathrm{P}})\boldsymbol{\sigma} + \boldsymbol{I}, \tag{5}$$

is a measure of the extra-stress which has the important property of being *symmetric positive definite*, thus it has a real matrix-logarithm. The matrix-logarithm transformation requires the diagonalization of the conformation tensor, $\boldsymbol{c} = \boldsymbol{Q}\boldsymbol{D}\boldsymbol{Q}^{\mathrm{T}}$, where $\boldsymbol{D}$ is the diagonal matrix of the eigenvalues and $\boldsymbol{Q}$ is the orthogonal matrix containing the eigenvector as vector column. The matrix-logarithm is interpreted as

$$\log(\boldsymbol{c}) = \boldsymbol{Q}\log(\boldsymbol{D})\boldsymbol{Q}^{\mathrm{T}}, \tag{6}$$

where the logarithm $\log(\boldsymbol{D})$ is applied component-wise. The evolution equation of the log-conformation is:

$$\frac{\partial \boldsymbol{s}}{\partial t} + \boldsymbol{u}\cdot\nabla\boldsymbol{s} - (\boldsymbol{\Omega}\boldsymbol{s} - \boldsymbol{s}\boldsymbol{\Omega}) - 2\boldsymbol{B} = \frac{f(e^{s})}{\lambda}e^{-s}, \tag{7}$$

where the $\boldsymbol{\Omega}$ and $\boldsymbol{B}$ are pure rotation and pure extension decompositions of the velocity gradient $\nabla\boldsymbol{u}$. Finally, the divergence of the viscoelastic extra-stress is recovered though the matrix-exponential of $\boldsymbol{s}$. This change of variable ensures by construction the positive definiteness of the conformation tensor. Fattal and Kupferman also showed that the numerical instabilities at high Weissenberg numbers are due to poor resolution of the exponential stress growth in time, and the exponential stress profile near geometrical singularities [17], with quadratic approximations. In the log-conformation representation, such exponential growths/profiles become linear and are accurately approximated by linear and quadratic schemes.

3.2. The pure streamfunction formulation

The main difficulty when solving the conservation equations (2)-(3) with the velocity and pressure as primary unknowns (***u***-*p* formulation), comes from the fact that there is no evolution equation for the pressure unknowns. Indeed, the pressure acts as a Lagrange multiplier of the incompressibility constraint which means that errors in the pressure fields directly link to errors in the conservation of mass. Most (if not all) viscoelastic algorithms use velocity-pressure fractional-step decoupling techniques, such as the SIMPLE, PISO or Chorin's projection methods [18-20]. The decoupling is achieved via an approximation of the inverse of the Jacobian matrix in the system of momentum equations. This approximation introduces a decoupling error; e.g. for the standard first order fractional-step method, the dominant error terms are proportional to $\Delta t/Re$ [21]. It means the decoupling technique is accurate at high *Re*, i.e. in flows driven by gravity or inertia, such as in aero-dynamics or hydro-dynamics problems. However, at low *Re* (especially below unity), the decoupling errors becomes very large. These flows are generally driven by pressure gradients, so that the velocity

and pressure fields are strongly coupled. As a result, the decoupling techniques may not be the most suitable.

Alternatives to the ***u*-*p*** formulation solve the momentum equation in its rotational form, where a transport equation for the vorticity $\boldsymbol{\omega} = \nabla \times \boldsymbol{u}$ is derived [22], e.g. the ***u*-*ω*** formulation and the ***ψ*-*ω*** formulation. As a result, the pressure unknowns are eliminated from the system of equations. Here we use a more robust formulation, the *pure-streamfunction formulation*, recently introduced by Kupferman [10] and by Chang, Giraldo and Perot [11], independently. It also uses the rotational form of the momentum equation, but all the kinematic unknowns are expressed in terms of a streamfunction $\boldsymbol{\psi}$, defined as a vector potential of the velocity field:

$$\boldsymbol{u} = \nabla \times \boldsymbol{\psi}, \tag{8}$$

and linked to the vorticity by a Poisson equation:

$$\boldsymbol{\omega} = \Delta \boldsymbol{\psi}. \tag{9}$$

The advantage of the pure-streamfunction formulation is that the continuity constraint is automatically fulfilled, by construction. In the 2D case, only one component of $\boldsymbol{\psi}$ is non-zero: $\boldsymbol{\psi} = (0, 0, \psi)$, therefore the streamfunction vector reduces to a scalar field φ, where

$$(u, v) = \nabla^{\perp} \psi = \left(-\frac{\partial \psi}{\partial y}, \frac{\partial \psi}{\partial x} \right). \tag{10}$$

Then, the evolution equation for the streamfunction scalar reads:

$$\frac{\partial}{\partial t} \Delta \psi + \left[\left(\nabla^{\perp} \psi \right) \cdot \nabla \right] \Delta \psi = \frac{\mu_S}{\rho} \Delta^2 \psi + \nabla \times \left(\nabla \cdot \boldsymbol{\sigma} \right), \tag{11}$$

In general, this formulation is more robust and accurate as it is fully implicit and does not produce errors. For details about the discretization procedure of the 4th order operators, see in reference [11].

4. Numerical examples

Our solution method for 2D viscoelastic flow was implemented in Matlab. We first test our algorithm for the simulation of Newtonian and viscoelastic flows at very low *Re* in the 4:1 contraction geometry, without free-surfaces. The geometry is discretised using a uniform orthogonal mesh, with 40 control volumes on the width of the downstream channel. The no-slip boundary condition is applied at the walls, and the fully-developed velocity and stress profiles are imposed at the inlet. We use an Oldroyd-B material with a viscosity ratio $\beta = \mu_S / (\mu_S + \mu_P) = 1/9$. The fluid is initially at rest, and after a short transient response the flow establishes a steady-state solution. In our calculation, the steady-state solution was found stable for $Wi < 4$, while a hydrodynamic instability developed from $Wi = 4$ and above. This instability is not a numerical instability since the simulation does not diverge. The streamlines are perturbed inside the downstream channel. Oscillations of the velocity in the spanwise direction partially separate the stress boundary-layers from the walls, as depicted in the figure 1. The flow perturbation was initiated near to the re-entrant corner and later propagated inside downstream. It is interesting to note that the perturbation started where the streamlines have high curvatures and the material experiences the largest shear deformation. This is an indication that this flow instability could correspond to a (physical) elastic instability [5].

To our knowledge, simulation results of unstable flows in the downstream channel have not been reported in the literature. However, our onset of instability at $Wi = 4$ quantitatively agrees with the non-linear stability analysis in [6], which predicts a subcritical elastic instability in the planar creeping Poiseuille flow of Oldroyd-B fluid occurring at *Wi* around 4. In their stability analysis, a perturbation of a few percentages in the wall shear stress is sufficient to make the flow unstable. The subcritical

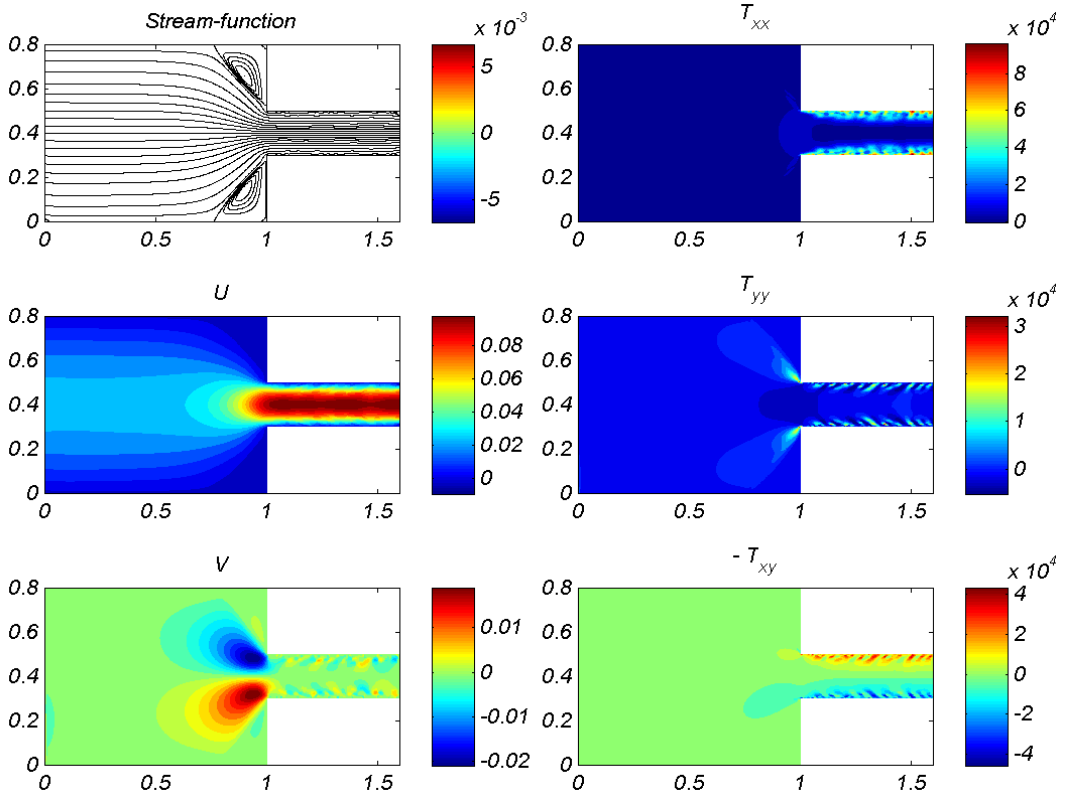

Figure 1. Snapshot of the streamlines, velocity and viscoelastic stress components of an unstable flow of Oldroyd-B material in a 4:1 contraction, at $Wi = 4$, $Re = 10^{-3}$ and $\beta = 1/9$.

elastic instability is also identified in [25,26] as an intrinsic mechanism of *melt fracture* defect in polymer extrusion, without stick-slip phenomena. The experimental investigation in [26] estimates the onset of the extrusion defect at $Wi = 4.6 \pm 0.6$, in cylindrical geometries. This empirical threshold value is also in good agreement with the results of our simulation.

The viscoelastic flow solver has further been coupled with a VOF solver, in order to simulate free-surfaces problems. Preliminary simulations of die-exit flows in planar extrusion were done. Figure 2 shows a snapshot of the free-surface during a simulation of extrusion for a Giesekus material, with the parameters $\alpha = 0.02$, $\beta = 0.5$, $Wi = 2$ and $Re = 1.25 \cdot 10^{-4}$. The maximum CFL number was set to 0.4. Only half of the domain was simulated, due to symmetry. In this particular flow, the swelling ratio of the planar extrudate is $\Lambda = H_{\text{extrudate}}/h_{\text{slit}} = 1.29$.

5. Final remarks

Historically, the high Weissenberg number problem has been addressed by developing stabilizing numerical techniques, adding an artificial diffusion to enhance the elliptic operator in the governing equations [19,20,23,24]. However, one may legitimately question whether the use of stabilizing techniques to avoid artificial instabilities does not produce an *artificial stability*. In our method, stabilisation techniques are not used; numerical stability is obtained by the log-conformation change of variable, and the fully-implicit pure-streamfunction formulation. These two reformulations increase the robustness of the numerical method, making it possible to simulate elastic instabilities. The accuracy of the results in the case of a turbulent flow is difficult to assess, because the whole range of spatial and temporal scales of the turbulences might not be resolved with the relatively coarse mesh. However, the prediction of the threshold Wi at which elastic instabilities are initiated is in good agreement with the previous analytical and experimental estimations. Further investigations need to be done on the critical amplitude of perturbation that triggers the subcritical elastic instability.

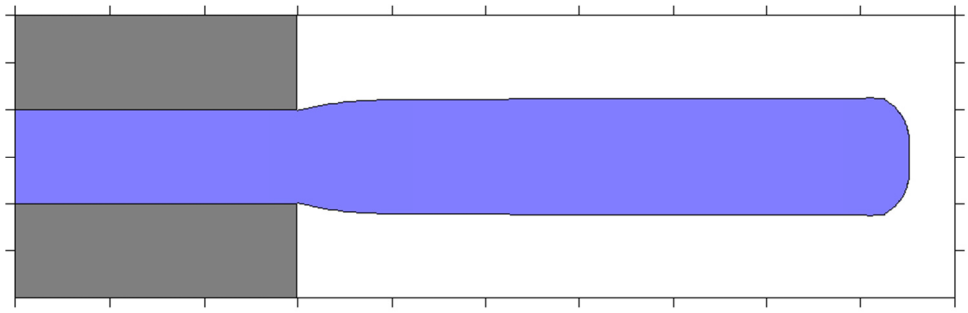

Figure 2. Numerical simulation of the planar extrusion die-exit flow of a Giesekus material, with $\alpha = 0.02$ and $\beta = 0.5$, at $Wi = 2$ and $Re = 1.25 \cdot 10^{-4}$.

To our knowledge, numerical simulation of extrusion melt-fracture defects has not been reported in the literature yet, and will be the subject of our future work. Our numerical method is also suitable to simulate interfacial deformations in the co-extrusion of different materials.

Acknowledgements
The authors would like to acknowledge the support of the Scientific Research Councils on Technology and Production Sciences (FTP) (Contract No. 09-072888, OPTIMAC), which is part of the Danish Council for Independent Research (DFF).

References
[1] Bird R B and Wiest J M 1995 *Annu. Rev. Fluid Mech.* **27** 169-93
[2] Pakdel P and McKinley G H 1996 *Phys. Rev. Lett.* **77** 2459-62
[3] Groisman A and Steinberg V 2000 *Nature* **405** 53-5
[4] Groisman A and Steinberg V 2004 *New J. Phys.* **6** 29-48
[5] Morozov A N and van Saarloos W 2007 *Phys. Rep.* **447** 112-43
[6] Meulenbroek B, Storm C, Morozov A N and van Saarloos W 2004 *J. Non- Newtonian Fluid Mech.* **116** 235-68
[7] Keunings R 1986 *J. Non- Newtonian Fluid Mech.* **20** 209-26
[8] Fattal R and Kupferman R 2004 *J. Non- Newtonian Fluid Mech.* **123** 281-5
[9] Fattal R and Kupferman R 2005 *J. Non- Newtonian Fluid Mech.* **126** 23-37
[10] Kupferman R 2001 *SIAM J. Sci. Comput.* **23** 1-18
[11] Chang W, Giraldo F and Perot J B 2002 *J. Comput. Phys.* **180** 183-99
[12] Keunings R 1986 *J. Comput. Phys.* **62** 199-220
[13] Rasmussen H K and Hassager O 1999 *J. Non- Newtonian Fluid Mech.* **82** 189-202
[14] Hirt C W and Nichols B D 1981 *J. Comput. Phys.* **39** 201-225
[15] Alves M A, Oliveira P J and Pinho F T 2003 *Int. J. Numer. Meth. Fluids* **41** 47-75
[16] Pilliod J E and Puckett E G 2004 *J. Comput. Phys.* **199** 465-502
[17] Rallison J M and Hinch E J 2004 *J. Non- Newtonian Fluid Mech.* **116** 141-62
[18] Oliveira P J, Pinho F T and Pinto G A 1998 *J. Non- Newtonian Fluid Mech.* **79** 1-43
[19] Xue S C, Tanner R I and Phan-Thien N 2004 *J. Non-Newtonian. Fluid Mech.* **123** 33-58
[20] Fiétier N and Deville M O 2003 *J. Comput. Phys.* **186** 93-121
[21] Perot J B 1993 *J. Comput. Phys.* **108** 51-8
[22] Gresho P M 1991 *Annu. Rev. Fluid Mech.* **23** 413-53
[23] Sureshkumar R and Beris A N 1995 *J. Non- Newtonian Fluid Mech.* **60** 53-80
[24] Baaijens F P T 1998 *J. Non- Newtonian Fluid Mech.* **79** 361-85
[25] Meulenbroek B, Storm C, Bertola V, Wagner C, Bonn D and van Saarloos W 2003 *Phy. Rev. Lett*. **90** 024502
[26] Bertola V, Meulenbroek B, Wagner C, Storm C, Morozov A, van Saarloos W and Bonn D 2003 *Phy. Rev. Lett*. **90** 114502